Multi-fidelity Analyses of Rotor Loads of Floating Offshore Wind Turbines with Wind/Wave Misalignment

Multi-fidelity Analyses of Rotor Loads of Floating Offshore Wind Turbines with Wind/Wave Misalignment

A. Ortolani[1], F. Papi[2], A. Bianchini[2], G. Persico[3], J. Drofelnik[4] and M.S. Campobasso[1]

[1] Department of Engineering, Lancaster University, Gillow Avenue, LA1 4YW Lancaster, UK
[2]Department of Industrial Engineering, University of Florence, Via di Santa Marta 3, 50139 Florence, Italy
[3]Dipartimento di Energia, Politecnico di Milano, Via Lambruschini 4, 20156 Milano, Italy
[4]Pipistrel Vertical Solutions d.o.o., Vipavska cesta 2, SI-5270 Ajdovcina, Slovenia

Email: m.s.campobasso@lancaster.ac.uk

Abstract. Reliable predictions of the aero- and hydrodynamic loads of fixed-bottom and floating offshore wind turbines are paramount for assessing fatigue life and designing load and power control systems. However, significant uncertainty affecting aerodynamic predictions still exists. This study presents cross-comparative analyses of the predictions of aerodynamic loads and power of fixed-foundation and floating wind turbine rotors with and without yaw errors using time- and frequency-domain Navier-Stokes Computational Fluid Dynamics, and the Blade Element Momentum theory. The considered test case is the National Renewable Energy Laboratory 5 MW reference turbine, assumed to be mounted in the floating case on a semi-submersible platform and undergoing pitching motion about the tower base. Although the overall qualitative agreement of the low- and high-fidelity predictions is found to be fair in all cases, for the considered regimes the agreement between the two methods is better for the pitching rotor in aligned wind than for the yawed flows regardless of the tower motion.

1. Introduction

The successful operation of floating offshore wind turbines (FOWTs) over lifetimes of 25+ years poses complex analysis and design challenges not encountered by fixed-bottom wind turbines (FBWTs), some of which stem from FOWT rotor unsteady aerodynamics [1,2]. FOWT overall system stability and loads depend on the interaction of a) hydrodynamic loads on the platform due to surface gravity waves and marine currents, b) rotor, nacelle and tower aerodynamic loads, and c) restoring loads due to platform mooring lines. Resolving with adequate reliability the underlying multi-disciplinary load-driving physics is also key to FOWT control design. Moreover, the development of FOWT wind farms also requires analyzing the generation process [3] and the propagation characteristics [4] of FOWT wakes, which may differ from those of FBWTs. The study of [3] also investigated the extent of compressible flow effects in FOWT rotor performance, a phenomenon previously found to be negligible in large FBWTs [5].

Both industrial and academic FOWT research often uses low-fidelity engineering codes, such as those adopting the Blade Element Momentum Theory (BEMT) for rotor aerodynamics. Questions

exist as whether these codes, initially developed for FBWTs, can adequately account for the more complex FOWT aerodynamics resulting from the additional entrainment velocities due to the platform motion, and wind/wave misalignment. To provide answers to this question, several research groups began cross-comparisons of FOWT aerodynamics using low-fidelity codes and high-fidelity Navier-Stokes (NS) Computational Fluid Dynamics (CFD), with the high-fidelity analyses increasingly becoming multi-disciplinary [6,7], i.e. adopting CFD to resolve both rotor aerodynamics and platform hydrodynamics in a fully coupled fashion. Extensive code-to-code comparisons are also the topic of Task 30 of the International Energy Agency.

FOWTs experience a wide range of metocean conditions, resulting in large variations in their operating regimes. A large number of these needs to be assessed for FOWT certification; it is thus expected that the agreement of low- and high-fidelity analyses may vary significantly over the set of regimes. Moreover, it is important to verify the fidelity of each component of the multi-fidelity analysis system. A parametric study of the BEMT and CFD methods for FOWT rotor aerodynamics was presented in [8], which used the AeroDyn BEMT code embedded in the NREL OpenFAST wind turbine engineering code [9] and the nonlinear frequency-domain harmonic balance (HB) compressible NS CFD code COSA [10] for the BEMT/CFD cross-comparison of loads and power for a 5 MW pitching rotor with no wind/wave misalignment, i.e. with pitching motion and wind direction contained in the vertical plane through the rotor axis. Fairly good agreement of BEMT and CFD was reported, although the CFD results were not compared to other verification or validation sources.

The principal aim of this study is to provide new reference CFD results of realistic pitching FOWT rotor aerodynamics supported by a three-code cross-verification/validation. The selected pitching FOWT configuration is the NREL 5MW reference turbine mounted on a semi-submersible platform. Hydrodynamics is not considered in the present study, and CFD and BEMT results are compared in simulations with imposed pitching motion, with and without yaw errors to mimic the effects of wind-wave misalignment. The main objectives of the study are to: a) characterize the dependence of FOWT power and loads on possible yaw errors (wind/wave misalignment), and b) analyze and quantify the correlation between the results of the BEMT and CFD analyses as the wind/wave misalignment increases.

2. Computational aerodynamics

The three Reynolds-averaged NS (RANS) CFD codes of this study are ANSYS FLUENT [11] and Lancaster's ARCTIC incompressible time-domain (TD) and HB codes [12], whereas the low-fidelity BEMT code is the AeroDyn BEMT code embedded in OpenFAST [9].

2.1. ARCTIC Time-domain and harmonic balance solvers

The finite volume ARCTIC codes solve the density-based form of the incompressible flow equations using a generalized artificial compressibility method; they use Menter's two-equation k-ω shear stress transport (SST) model for the turbulence closure. As its compressible flow counterpart [12], ARCTIC uses structured multi-block grids, discretizes the convective fluxes of both RANS and SST equations with a second order upwind scheme, and uses second order centered finite differences for both the diffusive fluxes and the space derivatives in the SST source terms. A space-discretization of the same type applied to unstructured grids is used for the FLUENT simulations herein. The TD and HB ARCTIC solvers can solve rotor flows in the rotor (relative) frame, or the stationary (absolute) frame. All CFD simulations herein are unsteady, and are performed in the absolute frame, with ARCTIC using a dual-time-stepping time integration [13] and FLUENT using the SIMPLEC algorithm [11].

The nonlinear frequency-domain HB RANS solution of wind turbine periodic flows can substantially reduce the analysis runtime with respect to that of conventional TD CFD. Nonlinear frequency-domain RANS CFD for wind turbine aerodynamics and/or aeroelasticity has been successfully demonstrated in several studies [14,15,16], including those with ARCTIC and COSA [12,10,17]. The COSA HB solver was shown to solve yawed wind turbine flows up to 30 times more rapidly than the COSA TD solver, with negligible loss penalties, in [17]. In the HB framework, the

sought periodic flow is written as a truncated Fourier series retaining only the first few complex harmonics whose frequency is a multiple of the known fundamental frequency of the excitation. The lower runtime of the HB solver is due to the fact that one solves directly for the periodic flow of interest, bypassing the solution of the time-dependent transient when solving in the TD.

2.2. OpenFAST blade element momentum theory set-up

The low-fidelity simulations below use OpenFAST version 3.0.0 dev (Jan. 2022) incorporating the AeroDyn BEMT module, and the ElastoDyn module for computing the rigid motion of the structure. The simulations are carried out using the rigid body model for all FOWT components by disabling all structural flexibility input in ElastoDyn, but enabling the rigid body motion of the platform. As discussed in [8], the motion of the tower is prescribed, adopting an ad-hoc procedure to enforce the desired tower motion. The publicly available model of the NREL 5MW wind turbine mounted on the OC4 DeepCWind Semi-Submersible is used.

Tower aerodynamics is not modelled in this study. To account for the rotor flow unsteadiness due to the platform motion, the Dynamic Blade Element Momentum Theory (DBEMT) is used in AeroDyn. DBEMT is obtained by using a dynamic wake model, i.e. including in the balance equations a time-derivative of the induction factors to account for the delay of the wake in adjusting to unsteady rotor loads [18]. The effects of local inflow skew, wind shear, turbulence, and tower flow disturbances can also be included in the analysis, but only the local skew due to yaw has been activated in part of the OpenFAST simulations presented below.

In AeroDyn, Glauert's empirical correction with Buhl's modification replaces the linear momentum balance at high axial induction factors. Three-dimensional flow features are modelled by using Prandtl tip and hub loss corrections and the Pitt-Peters skewed wake correction model. Modelling of airfoil unsteady aerodynamics relies on the Beddoes-Leishman unsteady model [18], activated by selecting the Hansen-Gaunaa-Madsen formulation. This formulation corrects airfoil lift and drag data accounting for unsteady attached flow aerodynamics, trailing and leading edge separations, and dynamic stall. Since in FOWT aerodynamics the angles of attack undergo periodic variations and may exceed the static stall limit, this formulation has been used in this study.

3. Rotor grid configuration and CFD set-up

The considered pitching FOWT is based on the NREL 5 MW reference turbine, which has tower height of 90 m and rotor diameter of 126 m; the rotor has an overhang of 5 m, a shaft tilt of 5^o and pre-coning of 2.5^o. Of these three features, only rotor pre-coning has not been accounted for in the simulations below.

The rotor geometry and the selected wall boundary conditions are reported in the left schematic of Fig. 1, and the grid around the airfoil at 50 percent tip radius is depicted in the right image of Fig. 1. The physical domain of the ARCTIC simulations is cylindrical, with the rotor center on the cylinder centerline 10 rotor radii from the inlet circular boundary at the front, 20 radii from the outlet circular boundary at the back, and 11 radii from the cylindrical far field boundary. The underlying principles for the choice of rotor domain sizes are discussed in [3]. Characteristic far field boundary conditions are enforced on all far field boundaries. The computational grid has 12,312,576 cells, with 129 grid nodes around each blade section (airfoil) and 129 nodes along the blade length. The distance of the first grid nodes off the wall boundaries (blades and hub) from such boundaries results in a y+ value of about 1 in all presented simulations. A butterfly mesh scheme is adopted around the rotor centerline to prevent the formation of degenerate cells. It has been verified that this grid provides mesh-independent rotor performance and load parameters.

The grid adopted for all FLUENT simulations is that used in [3] and [8]; it was shown to provide mesh independent solutions in [3]. It differs from the ARCTIC grid only in that it has 9,879,552 cells. The overall cell count reduction compared to the ARCTIC grid is because the FLUENT grid uses only 65 nodes along the blade length. It has been verified that this difference results in negligible differences of rotor forces and moments using either grid with both FLUENT and ARCTIC.

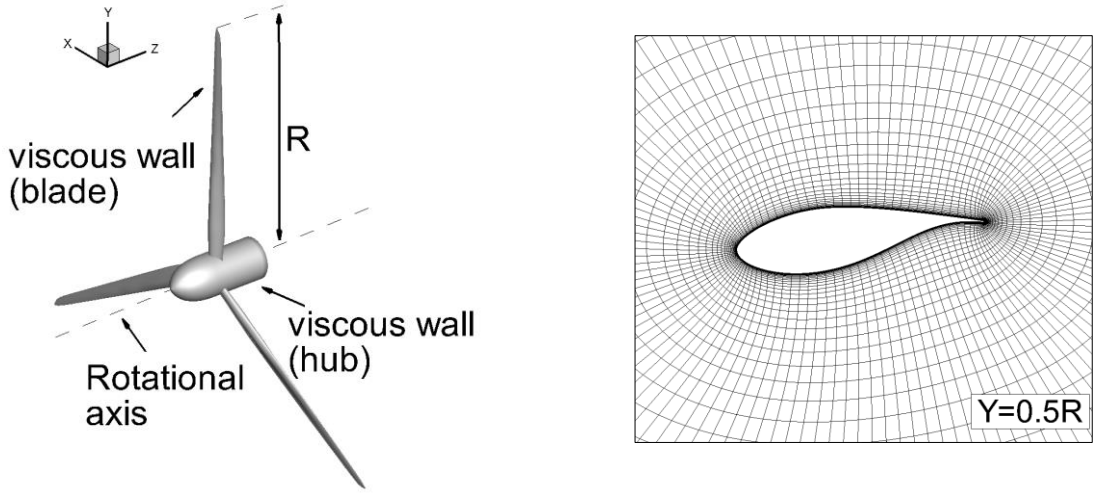

Figure 1. NREL 5 MW rotor geometry (left), and airfoil grid at 50 percent tip radius (right).

4. FBWT and FOWT configurations

All positive axis and angle conventions are indicated in Fig. 2. The top and front views of the FBWT are depicted, respectively, in the left and middle schematics. The segments labeled B1, B2, B3 denote the blade axes, and the angle θ_r denotes the time-dependent angular position of the reference blade B1, given by $\theta_r=\Omega_r t$, with Ω_r being the rotor angular speed. The wind/wave misalignment, i.e. the angle between wind speed and direction of wave propagation (in this study, the latter direction is always in the vertical plane containing the rotor axis), is denoted by β. As all unsteady simulations are carried out in the absolute frame, the position of the xyz system, whose origin is the rotor center of the FBWT, does not change during either the FBWT or FOWT analyses. The side view of the considered pitching FOWT is reported in the right schematic of Fig. 2, where Ω_p denotes the angular frequency of tower pitching. The time-dependent inclination of the tower is $\theta_p=\Theta_p \sin(\Omega_p t+\varphi_p)$, where Θ_p is the user-given tower pitching amplitude, and φ_p is the initial phase between rotor and tower angular positions, which remains constant when Ω_r is an integer multiple of Ω_p. The mathematical formulation of grid displacements and velocities resulting from the composition of rotor rotation and tower pitching implemented in ARCTIC and COSA is in [3].

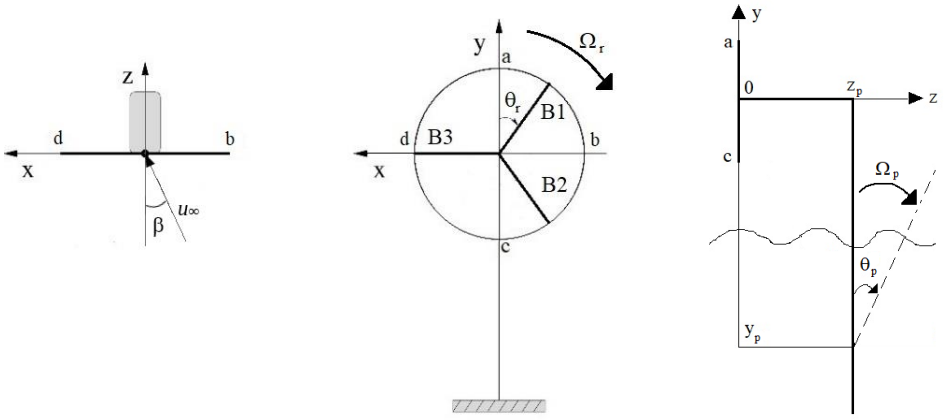

Figure 2. Top view (left schematic) and front view (middle schematic) of FBWT, and side view of pitching FOWT (right schematic).

All analyses herein use a close-to-rated wind speed of 11 m/s and a rotor speed of 12 RPM, corresponding to a frequency of 0.2 Hz. The effect of rotor tilt is accounted for by inclining the oncoming wind by 5° upwards on the rotor axis (z axis). In the FOWT analyses, φ_p=0°; the vertical coordinate y_p=-90 m of the pitching center equals that of the tower base, and z_p=5 m is used to account for the rotor overhang. This choice is representative of semi-submersible FOWT platforms.

The FOWT simulations herein use pitching frequency of 0.1 Hz. This value lies within the broader frequency range that is typically excited by irregular ocean waves during operation [19]. For instance, a peak spectral period of 10s, a significant wave height of 6 m and a mean wind speed of 11.4 m/s are used in the basin tests in [20] to model operation in rough sea states. In deep- to mid-depth waters, where FOWTs are expected to operate, waves are typically far from their breaking limit and linear theory can describe wave-induced motions [19]. Although non-linear effects such as viscous drag need to be accounted for when modelling FOWT hydrodynamics, in the first instance one may assume that the frequency response of the structure is mostly linear and is close to the wave excitation frequency. Moreover, the pitching frequency of 0.1 Hz has been used in other recent FOWT CFD studies [4,8], and, to enable cross-comparison of this study's results with others in the literature, it has been decided to continue using this same frequency.

5. Results

Here, the simulations of FLUENT, ARCTIC TD and HB, and OpenFAST/AeroDyn are cross-compared for selected FBWT and pitching FOWT regimes to a) examine the quantitative and qualitative dependence of the periodic cycles of rotor thrust and power, and blade out-of-plane bending moments on the flow regime, and b) analyze the correlation of low- and high-fidelity analyses for different types of flow regimes. Both FLUENT and the ARCTIC TD simulations use a time-step corresponding to one degree of rotor revolution. All ARCTIC HB analyses use 4 complex harmonics (HB4). Four regimes are considered: 1) rigid foundations and no wind misalignment, 2) rigid foundation and yaw error β=20°, 3) pitching rotor with $2\pi\Omega_p = 0.1$ Hz and Θ_p=1° with no wind/wave misalignment, and 4) pitching rotor with $2\pi\Omega_p = 0.1$ Hz and Θ_p=1° with wind/wave misalignment β=20°, whereby the direction of wave propagation is parallel to the rotor axis but the wind has yaw error of 20°. All four regimes also include the rotor tilt of 5°, so that regime 1 is affected by low-level unsteadiness. The hub radius has been set to 5 m in the BEMT analyses for consistency with the CFD rotor model.

5.1. Comparative analysis of rotor thrust and power

The cyclic profiles of thrust T and power P of blade 1 obtained with the CFD and BEMT codes for the FBWT operating with β=20° are reported in Fig. 3. The left plot compares the low- and high-fidelity periodic profiles of the blade thrust, and the right plot compares those of the blade power. The variable t/T on the x-axis of both plots is a nondimensionalized time variable used to plot the evolution of the considered output from the start to the end of one periodic cycle, and the symbol T denotes the period of one rotor revolution. Reference blade B1 is vertical and above the hub at the cycle start. In this and all other analyses below, the positive sign of the prescribed β corresponds to the indication in the left schematic of Fig. 2, whereas the prescribed rotor speed Ω_r is negative with respect to the positive convention in the middle schematic of Fig. 2. Due to these prescribed conditions, the maximum angles of attack (AoAs) to blade B1 are expected to occur for 180°< Θ_r<270°, which is part of the windward trajectory of blade B1.

Very good agreement of the two CFD T and P estimates of Fig. 3 is noted, whereas notable differences between the CFD and BEMT analysis are observed, particularly in the P profiles. The BEMT analysis overestimates the amplitude of the T and P profiles, moderately overestimates the mean value of T, and underestimates the mean value of P. Notable phase differences between the BEMT and CFD profiles also exist. Both CFD and BEMT predict that the peak power occurs after the peak thrust. However, the BEMT peaks occur earlier in the rotor revolution than the CFD peaks. Moreover, the phase error on the P peak is significantly larger than that on T, pointing to significant

differences in the resolution of yawed flow physics of the two methods. Inspection of the P profiles of Fig. 3 also highlights that the BEMT profile has a harmonic shape, pointing to a seemingly linear response to the yawed condition, whereas the CFD profile has a periodic but non-harmonic profile, indicating the response contains also flow harmonics with frequency higher than that of the rotor speed. This is also confirmed by the fact that the ARCTIC P profile obtained with a single flow harmonic analysis, not reported for brevity, differs significantly from the FLUENT P profile.

It is noted that the FLUENT solution has achieved periodicity, and the ARCTIC HB solution is periodic by construction.

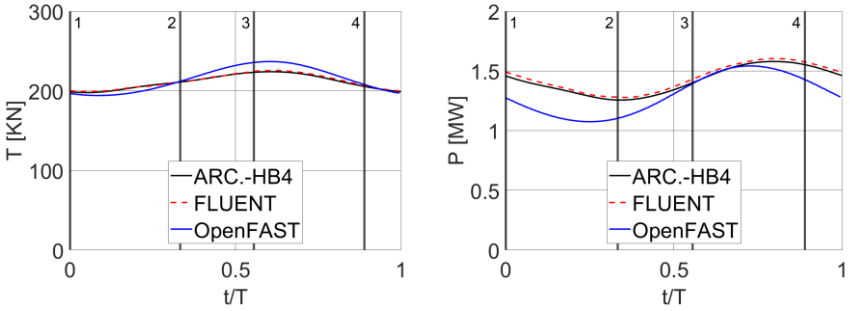

Figure 3. ARCTIC HB4, FLUENT and OpenFAST/AeroDyn predictions of periodic profiles of blade thrust T (left) and power P (right) for rigid foundations and β=20°.

The T and P cyclic profiles of the entire rotor obtained with ARCTIC TD and HB4, FLUENT and OpenFAST for the FOWT operating with β=0° are reported in Fig. 4. In this and the next FOWT analysis, the prescribed Ω_p is positive with respect to the convention in the right schematic of Fig. 2. The phase φ_p between the rotor revolution and the tower pitching cycle is zero, and therefore $\theta_p = \theta_r = 0$ at the start of each pitching cycle, a time at which blade B1 is vertical and above the hub. The pitching cycle takes two rotor revolutions, hence the maximum of t/T is 2.

Good agreement of the three CFD analyses is observed. The BEMT and CFD profiles of the rotor thrust have the same shape, but the BEMT mean value is higher. Good qualitative and quantitative agreement is instead observed between the BEMT and CFD rotor power predictions. The ARCTIC TD and FLUENT solutions have achieved periodicity. Excellent agreement of ARCTIC TD and HB4 is noted.

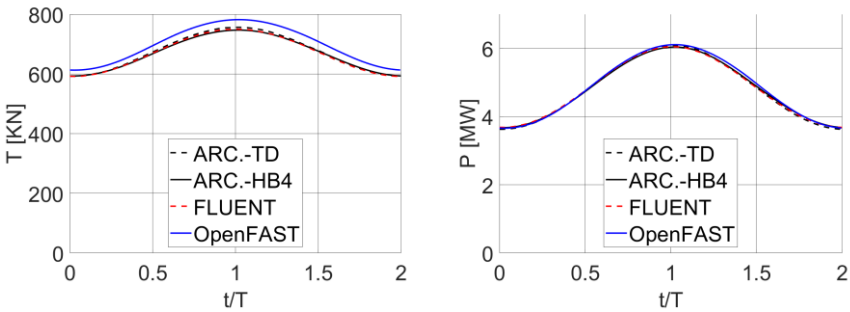

Figure 4. ARCTIC TD and HB4, FLUENT and OpenFAST/AeroDyn predictions of periodic profiles of rotor thrust T (left) and power P (right) for pitching platform and β=0°.

The cyclic profiles of T and P of the entire rotor obtained with ARCTIC TD and HB4, FLUENT and OpenFAST for the FOWT operating with β=20° are reported in Fig. 5. All analyses use again $\varphi_p=0$, so that $\theta_p = \theta_r = 0$ at the start of each pitching cycle, when blade B1 is vertical and above the hub. Also in this case, good agreement of the three CFD analyses is noted. The BEMT T profile is in good agreement with the CFD predictions, whereas the BEMT P profile is lower than the CFD estimate. Cross-comparing Figures 4 and 5 indicates that BEMT predicts larger reductions of FOWT P due to

wind misalignment than CFD does, and that it predicts higher T peaks than CFD for the FOWT problem at β=0º. The higher rotor thrust predicted by BEMT for β =0º is also consistent with the higher out-of-plane blade bending moments for this regime observed below.

The FLUENT T and P profiles have achieved periodicity, but the ARCTIC TD profiles have not yet. Hence, some uncertainty still affects this ARCTIC TD result.

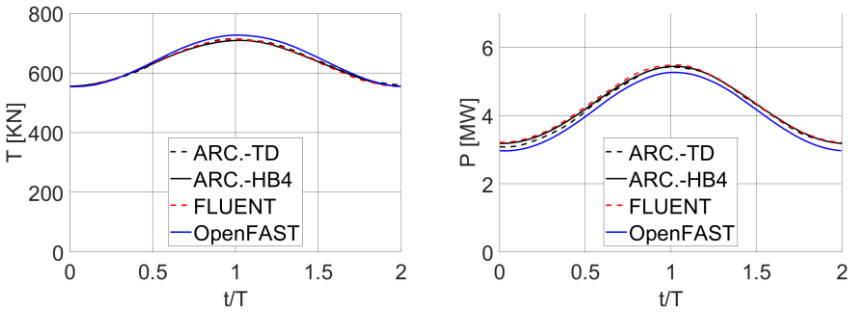

Figure 5. ARCTIC TD and HB4, FLUENT and OpenFAST/AeroDyn predictions of periodic profiles of rotor thrust T (left) and power P (right) for pitching platform and β=20º.

The mean and maximum values of T and P computed with all codes are reported in Tables 1 and 2, respectively. For reference, the second and third columns of both tables also report the results for the FBWT with β=0º. The results of the mean outputs presented in Tab. 1 show that the BEMT analysis overpredicts the CFD estimate of T in all cases, with a maximum overprediction of 4.2% with respect to the ARCTIC HB4 result for the FOWT with β=0º. There is not a clear trend of over-/underpredictions of P between the BEMT and CFD analyses. The maximum differences between BEMT and CFD P estimates are observed with wind misalignment, with a difference of 4.7% of the BEMT and ARCTIC HB4 power for the FBWT. As expected, the FLUENT P estimate for the FBWT at β=0º is lower than those obtained with the same grid and a steady simulation (no shaft tilt) in [3].

The trends of Tab. 2 are similar to those discussed for the mean values in Tab. 1, but some differences are slightly larger. For example, the BEMT overprediction of the peak thrust over the CFD estimates for the FOWT with β=0º is 4.7%,

Table 1. OpenFAST/AeroDyn, ARCTIC TD and HB4, and FLUENT mean values of rotor thrust T [KN] and rotor power P [MW] for examined FBWT and pitching FOWT cases.

	FBWT - β=0º		FBWT - β=20º		FOWT - β=0º		FOWT - β=20º	
	T	P	T	P	T	P	T	P
FAST	701.2	4.85	643.3	4.06	699.3	4.87	642.0	4.09
ARC TD	---	---	---	---	674.7	4.82	635.0	4.24
ARC HB4	671.0	4.79	633.1	4.25	671.0	4.83	633.0	4.28
FLUENT	671.1	4.79	635.5	4.31	671.0	4.83	633.5	4.32

Table 2. OpenFAST/AeroDyn, ARCTIC TD and HB4, and FLUENT peak values of rotor thrust T [KN] and rotor power P [MW] for examined FBWT and pitching FOWT cases.

	FBWT - β=0º		FBWT - β=20º		FOWT - β=0º		FOWT - β=0º	
	T	P	T	P	T	P	T	P
FAST	701.2	4.85	643.4	4.07	781.7	6.11	726.6	5.26
ARC TD	---	---	---	---	756.0	6.08	713.8	5.42
ARC HB4	671.3	4.80	634.5	4.26	747.0	6.04	708.9	5.44
FLUENT	672.1	4.80	637.0	4.33	749.8	6.05	712.0	5.48

5.2. Comparative analysis of blade out-of-plane bending moment

The out-of-plane bending moment (BM) of the three blades predicted by all simulations of the considered regimes are depicted in Figures 6, 7 and 8. The considered BM is calculated with respect to the axis contained in the rotor plane, normal to the blade axis and passing through the rotor center. The blade counting indicated in all three figures is that indicated in the middle schematic of Fig. 2.

Figure 6, referring to fixed foundations and yaw error of 20°, highlights that the BEMT analysis notably overpredicts peak BMs with respect to available CFD predictions. The BEMT and CFD predictions of both the phase between the BM cycles and the blade azimuthal positions, and the BM minima are in good agreement.

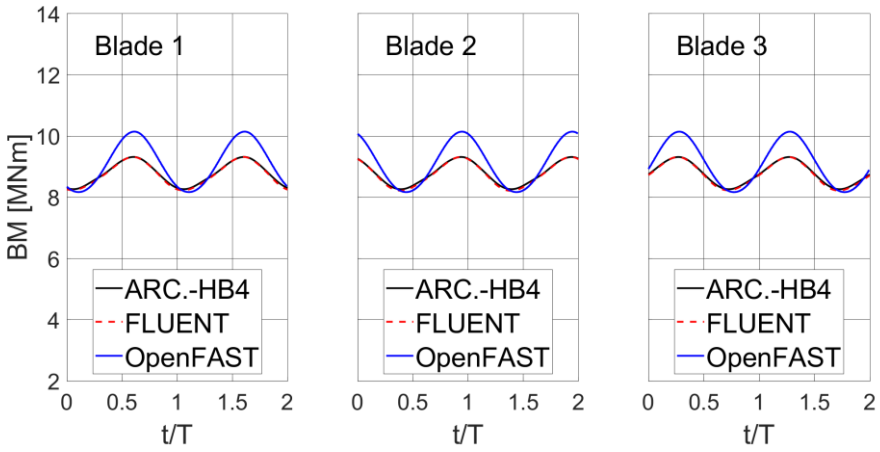

Figure 6. ARCTIC HB4, FLUENT and OpenFAST/AeroDyn predictions of periodic profiles of the out-of-plane bending moment BM on the blades for rigid foundations and β=20°.

Figure 7 refers to floating foundations and no wind/wave misalignment. As $\Omega_r=2\Omega_p$ and $\varphi_p=0$, all blades experience their maximum BM around t/T=1, when the tower top has maximum windward velocity. The maximum BM is experienced by blade 1, as this blade experiences the highest tower-induced entrainment velocity and angles of attack around t/T=1. Unlike the FBWT case with β=20°, the BEMT and CFD profiles for the FOWT at β=0° are fairly parallel along most parts of the pitching cycle, indicating similar physics capturing capabilities of both analysis methods. The maximum differences of the BEMT and CFD analyses, however, remain comparable to those of the FBWT case with wind misalignment.

Figure 8 refers to floating foundations and wind/wave misalignment of β=20°. The misalignment reduces again the correlation of BEMT an CFD profiles, as the two profile sets are no longer parallel over most of the pitching cycle. Cross-comparing the profiles of Figures 8 and 6 shows that the largest discrepancies between BEMT and CFD occur where the peak BMs of the FBWT are observed.

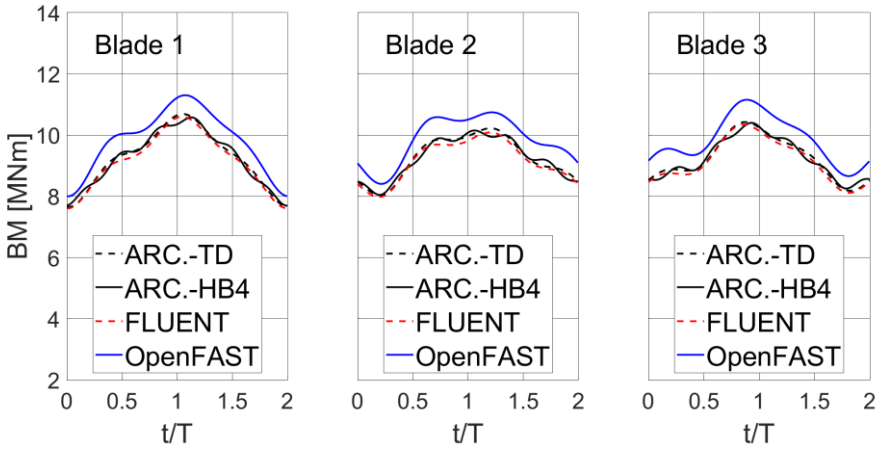

Figure 7. ARCTIC TF and HB4, FLUENT, and OpenFAST/AeroDyn predictions of periodic profiles of the out-of-plane bending moment BM on the blades for pitching platform and β=0°.

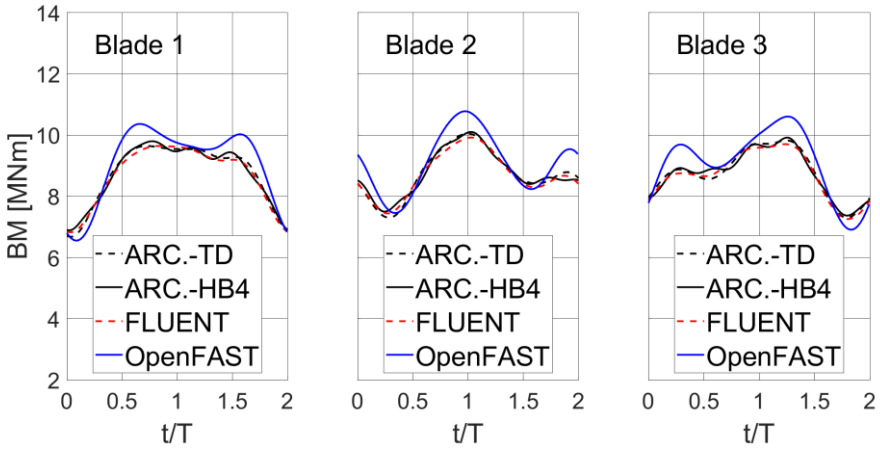

Figure 8. ARCTIC TD and HB4, FLUENT and OpenFAST/AeroDyn predictions of periodic profiles of the out-of-plane bending moment BM on the blades for pitching platform and β=20°.

Cross-comparing the BM profiles of Figures 6 and 7 indicates that the level of unsteadiness caused by the considered pitching motion is larger than that caused by the 20° wind misalignment, as the BM variations of the latter figure are larger than those of the former figure. For this reason, the BM patterns associated with the case of FOWT with wind/wave misalignment are closer to the BM profiles of the FOWT with β=0° than those of the FBWT with β=20°. In light of the observed level of agreement of BEMT and CFD for the misalignment and pitching regimes, it is expected that the overall reliability of BEMT predictions for FOWTs operating in misaligned wind will also depend on the relative magnitude of the aerodynamic unsteadiness due to yaw errors and platform motion.

It is also emphasized that a comprehensive comparison of BEMT and CFD predictions should examine both blade- and rotor-related outputs. For example, the T and P profiles of Fig. 5 indicate smooth profiles and good agreement of BEMT and CFD, whereas the higher pattern complexity of the BM profiles of Fig. 8 and the differences between BEMT and CFD predictions point to complex unsteady aerodynamics and different physics capturing capabilities of the two approaches. These differences may be hidden by phase cancellation when examining rotor-related outputs only.

A quantitative comparison of the blade out-of-plane BMs obtained with the BEMT-based and CFD analyses is provided in Tables 3 and 4. The former table provides the mean BM value of all blades for all considered regimes, whereas the latter table provides the maximum BM values. For reference, the FBWT BMs at $\beta=0^o$ are also reported. Taking the ARCTIC HB4 as a reference for the CFD simulations, the data of Tab. 3 show that the largest differences between BEMT and CFD predictions occur for the two $\beta=0^o$ cases, with differences of about 6.7% and 6.4% for the FBWT and FOWT case, respectively. With the $\beta=20^o$ misalignment, the difference between BEMT and CFD profiles in the cycle varies significantly, being large in the peak regions and fairly small elsewhere. Thus, the difference between the BEMT and CFD profiles is only about 3.8% for the FBWT and 3.6% for the FOWT. The BEMT/CFD differences of maximum BMs follow a different trend, with the largest difference of about 8.6% for the FBWT with $\beta=20^o$, and differences of 6.6% and 6.1% for the FOWT at $\beta=0^o$ and $\beta=20^o$, respectively.

Table 3. OpenFAST/AeroDyn, ARCTIC TD and HB4, and FLUENT mean values of out-of-plane bending moment BM [MNm] of all blades for examined FBWT and pitching FOWT cases.

	FBWT - $\beta=0^o$			FBWT - $\beta=20^o$			FOWT - $\beta=0^o$			FOWT - $\beta=20^o$		
	BM1	BM2	BM3	BM1	BM2	BM3	BM1	BM2	BM3	BM1	BM2	BM3
FAST	9.88	9.88	9.88	9.11	9.11	9.11	9.84	9.86	9.86	9.09	9.10	9.10
ARC TD	---	---	---	---	---	---	9.26	9.27	9.27	8.76	8.76	8.77
ARC HB4	9.26	9.26	9.26	8.78	8.78	8.78	9.25	9.26	9.26	8.77	8.77	8.78
FLUENT	9.17	9.17	9.17	8.75	8.75	8.75	9.17	9.17	9.18	8.71	8.71	8.72

Table 4. OpenFAST/AeroDyn, ARCTIC TD and HB4, and FLUENT peak values of out-of-plane bending moment BM [MNm] of all blades for examined FBWT and pitching FOWT cases.

	FBWT - $\beta=0^o$			FBWT - $\beta=20^o$			FOWT - $\beta=0^o$			FOWT - $\beta=20^o$		
	BM1	BM2	BM3	BM1	BM2	BM3	BM1	BM2	BM3	BM1	BM2	BM3
FAST	10.13	10.13	10.13	10.14	10.14	10.14	11.30	10.74	11.15	10.36	10.78	10.60
ARC TD	---	---	---	---	---	---	10.69	10.22	10.43	9.64	10.05	9.82
ARC HB4	9.40	9.40	9.40	9.32	9.32	9.32	10.58	10.15	10.40	9.80	10.10	9.92
FLUENT	9.36	9.36	9.36	9.32	9.32	9.32	10.60	10.09	10.34	9.64	9.92	9.70

To investigate the discrepancies between the CFD and BEMT predictions of integral loads and power observed in Figures 3 and 6 for the FBWT operating with yaw error of 20^o, the blade B1 radial profiles of normal force and power per blade length predicted by the two methods are plotted, respectively, in the left and right plots of Figure 9. Four azimuthal positions of blade B1, corresponding to four values of t/T, are considered; the positions labeled 'pos.1' to 'pos. 4' in Fig. 9 are those marked in the two plots of Fig.3. Inspection of the F_n profiles of Fig. 9 shows fair qualitative agreement of the two predictions. The quantitative agreement of the two predictions is acceptable below 60% of the blade tip radius, with the differences not varying significantly during the rotor revolution. Above this radius, however, the difference between the F_n predictions varies notably during the cycle: it is small at the cycle start (position 1), grows to a maximum at t/T=0.56, and decreases approaching the cycle end (position 4). This pattern is consistent with the blade integral of F_n reported in the left plot of Fig. 3.

Also the P profiles of Fig. 9 are consistent with their integral values in Fig. 3. The best agreement of the two P predictions is at t/T=0.56 (position 3). At the other three azimuthal positions, the agreement is quite poor, over most length of the blade, and is azimuthal position-dependent, with integral values consistent with those in Fig. 3.

All the differences above stem from different predictions of the flow velocity vector, magnitude and direction, at the blade leading edge, or, equivalently, from different predictions of the axial and

circumferential induction factors. As the differences between BEMT and CFD F_n profiles are smaller than those between the P profiles, it seems that the greater impact of the induction differences is on the local AoA differences, as small AoA variations affect the local thrust less than the tangential force. The overall thrust overestimate and power underestimate of BEMT over CFD would point to a BEMT underestimation of the local AoA in the blade outboard part. Thus, the BEMT predictions for yawed flows are less reliable than those of CFD, which was successfully validated against measurements [17]. This BEMT shortcoming also impairs the analysis of FOWTs with wave/wind misalignment.

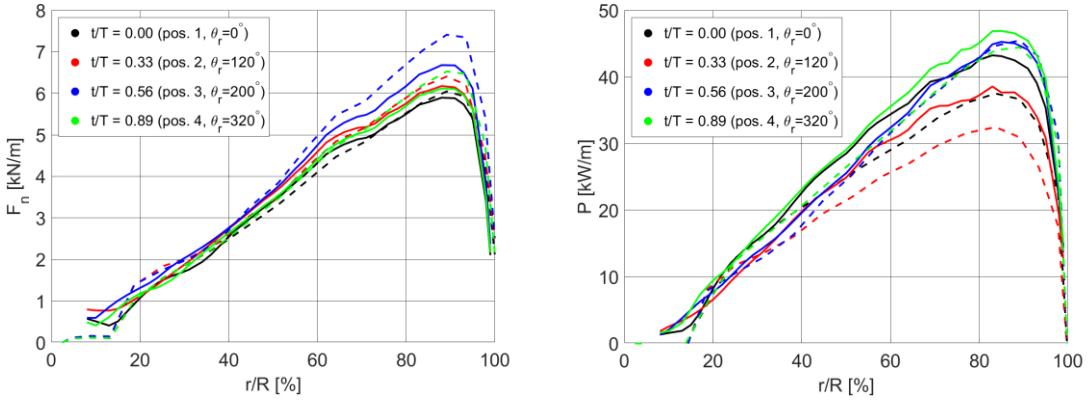

Figure 9. Comparative analyses of blade B1 radial profiles of normal force F_n (left) and power P (right) per unit blade length computed by ARCTIC HB4 (solid lines) and OpenFAST (dashed lines) simulations for rigid foundations and β=20°. Selected four azimuthal positions of blade B1 are those labeled 1 to 4 in Fig. 3.

6. Conclusions

A cross-comparative analysis of a FBWT and a pitching FOWT rotor in straight and yawed wind using the BEMT functionalities of OpenFAST, the ARCTIC TD and HB CFD solvers, and the ANSYS FLUENT CFD code was presented. The NREL 5 MW turbine rotor at close-to-rated wind speed and pitching with amplitude of 1° and frequency of 0.1 Hz was considered. Overall fair correlation of BEMT and CFD results was found, with estimates of both mean and maximum rotor thrust and power differing by up to about 5%, and estimates of maximum blade out-of-plane BMs differing by more than 8%. The largest differences between the BEMT and CFD cyclic BM profiles were observed for the condition of yawed wind, and the issue affects both FBWT and FOWT analyses.

The fact that the BM profiles predicted by the low- and high-fidelity approaches for the considered FOWT regime with zero yaw error are fairly parallel suggests that the BEMT model captures reasonably well the FOWT aerodynamics of the considered case. Conversely, the loss of parallelism with the introduction of a yaw error suggests the need for more significant improvements of the BEMT approach to yawed wind aerodynamics. The presented results also suggest that the reliability of the overall BEMT prediction of FOWT aerodynamics with wind misalignment may decrease when the flow unsteadiness induced by the yaw error approaches or outweighs that due to the platform motion.

Acknowledgments

This study was partly performed under the Project HPC-EUROPA3 (INFRAIA-2016-1-730897), with support of the EC Research Innovation Action under the H2020 Programme; Dr. Campobasso acknowledges the support of the Department of Industrial Engineering – University of Florence, including Professors Michele Marconcini, Roberto Pacciani and Andrea Arnone, and the computer resources and technical support of the CINECA HPC center. The project was also supported by the UK Engineering and Physical Sciences Research Council under Grant EP/T004274/1. Lancaster University is also acknowledged for the use of the HEC cluster for this study.

References

[1] Micallef D and Rezaeiha A 2021, Floating offshore wind turbine aerodynamics: Trends and future challenges, *Sustainable and Renewable Enery Reviews*, **152**: 111696.
[2] Sebastian T and Lackner M A S 2018, Characterization of the unsteady aerodynamics of offshore floating wind turbines, *Wind Energy*, **16**(3): 339-352.
[3] Ortolani A, Persico G, Drofelnik J, Jackson and Campobasso M S 2020, Computational Fluid Dynamics Analysis of Floating Offshore Wind Turbines in Severe Pitching Conditions, *Journal of Engineering for Gas Turbine and Power,* **142**(12).
[4] Lienard C, Boisard R and Daudin C 2019, Aerodynamic behavior of a floating offshore wind turbine, *AIAA SciTech Forum*, American Institute of Aeronautics and Astronautics.
[5] Campobasso M S, Yam M, Drofelnik J, Piskopakis A and Caboni M 2014, Compressible Reynolds-averaged Navier-Stokes analysis of wind turbine turbulent flows using a fully coupled low-speed preconditioned multigrid solver, *ASME Turbo Expo Technical Congress and Exposition*, ASME paper GT2014-25562
[6] Tran T-T and Kim D-H 2016, Fully coupled aerohydrodynamic analysis of a semi-submersible FOWT using a dynamic fluid body interaction approach, *Renewable Energy*, **92**: 244-261.
[7] Liu Y, Xiao Q, Incecik A, Peyrard C, Wan D 2017, Establishing a fully coupled CFD analysis tool for floating offshore wind turbines, *Renewable Energy*, **112**: 280-301.
[8] Ortolani A et al 2020, Cross-comparative analysis of loads and power of pitching floating offshore wind turbine rotors using frequency-domain Navier-Stokes CFD and blade element momentum theory *J. Phys.: Conf. Ser*. **1618**(5) 052016.
[9] Jonkman J and Sprague M 2022, OpenFAST: An aeroelastic computer-aided engineering tool for horizontal axis wind turbines, *National Renewable Energy Laboratory.* www.nrel.gov/wind/nwtc/openfast.html. Accessed on 19 January 2022.
[10] Campobasso M S, Drofelnik J and Gigante F 2016, Comparative Assessment of the Harmonic Balance Navier-Stokes Technology for Horizontal and Vertical Axis Wind Turbine Aerodynamics, *Computers and Fluids*, **136**: 354-370.
[11] Ansys-Inc. Fluent theory guide, release 2019.r3. www.ansys.com/products/fluids/ansys-fluent, 2019, Accessed on 19 January 2022.
[12] Cavazzini A, Campobasso M S, Marconcini M, Pacciani R and Arnone A 2019, Harmonic balance Navier-Stokes analysis of tidal stream turbine wave loads, *Recent Advances in CFD for Wind and Tidal Offshore Turbines*, Springer Tracts in Mechanical Engineering, ed E Ferrer and A Montlaur, Springer International Publishing.
[13] Campobasso M S, Piskopakis A, Drofelnik J, Jackson A 2013, Turbulent Navier-Stokes analysis of an oscillating wing in a power extraction regime using the shear stress transport turbulence model*, Computers and Fluids*, **88**: 136-155
[14] Horcas S G, Debrabandere F, Tartinville B, Hirsch C and Coussement G 2017, Rotor-tower interactions of DTU 10 MW reference wind turbine with a non-linear harmonic method, *Wind Energy*, **20**(4): 619-636.
[15] Howison J and Ekici K 2015, Dynamic stall analysis using harmonic balance and correlation based γ-Re_ϑ transition model for wind turbine applications, *Wind Energy*, **18**(12): 2047-2063.
[16] Naung S W, Rahmati M and Farokhi H 2021, Nonlinear frequency domain solution method for aerodynamic and aeromechanical analysis of wind turbines, Renewable Energy, **167**: 66-81.
[17] Drofelnik J, Da Ronch A and Campobasso M S 2018, Harmonic balance Navier-Stokes aerodynamic analysis of wind turbines in yawed wind, *Wind Energy*, **21**(7): 515-530.
[18] Hansen M O L 2015, Aerodynamics of wind turbines, 3rd edition, Routledge - Taylor & Francis.
[19] Faltisen O M 1990, Sea Loads on Ships and Offshore Structures, Campbridge University Press, Chapter 2, pp. 23-34.
[20] Robertson A et al 2014, Offshore Code Comparison Collaboration Continuation within IEA Wind Task 30: Phase II Results Regarding a Floating Semisubmersible Wind System, ASME paper OMAE2014-24040.